*29th EPS Conference on Plasma Phys. and Contr. Fusion Montreux, 17-21 June 2002 ECA Vol. **26B**, P-1.056 (2002)*

The effect of magnetic configurations on H-mode in MAST

H. Meyer, A. Kirk, L.C. Appel, E.R. Arends[†], P.G. Carolan, G.F. Counsell, G. Cunningham, A.R. Field, R. Martin, T.M. Pinfold, A. Tabasso, M.R. Tournianski, M. Valovič, M.J. Walsh[‡], and the MAST Team

EURATOM/UKAEA Fusion Association, Culham Science Centre, Abingdon, Oxfordshire, OX14 3DB, UK

[†]*FOM Instituut voor plasmafysica 'Rijnhuizen', Association EURATOM-FOM, Trilateral Euregio Cluster, Postbus 1207, 3430 BE Nieuwegein, The Netherlands*

[‡]*Walsh Scientific Ltd., Culham Science Centre, Abingdon, Oxfordshire, OX14 3EB, UK*

Introduction:

The ELMy H-mode is the reference scenario in ITER and a candidate regime for a future tokamak power plant. It is commonly observed in present day magnetic fusion devices [1, 2, 3, 4]. However, the influence of the magnetic configuration on the access to H-mode is one of the least understood subjects [5, 6, 7], and only a few theories based on fluid equations address this issue [8, 9]. In this framework, the position of the active X-point on the last closed flux surface (LCFS) with respect to the ion ∇B-drift is of particular importance. There are only a few devices with the appropriate up/down divertor geometry such as MAST, TCV, NSTX and DIII-D, which can study this effect without changing the direction of the toroidal field and plasma current or the recycling. Furthermore, these devices can also operate in double null diverted (DND) configurations rather than only in single null diverted (SND). In particular the effect of position of the X-points with respect to the ion ∇B-drift on H-modes has been investigated in detail on DIII-D [7, 10, 11].

In this paper we present a series of experiments on MAST investigating the influence of the magnetic configuration ($\delta = 0.37 \pm 0.01$, $\kappa = 1.9 \pm 0.05$) with respect to the degree of separatrix separation on the H-mode access in Ohmic ($I_p = (630 \pm 30)$ kA, $\bar{n}_e = (4.0 \pm 0.3) \cdot 10^{19}\,\mathrm{m}^{-3}$ – 50% of Greenwald density) discharges. Spherical tokamaks, such as MAST, show stronger neoclassical effects because of the stronger magnetic field curvature due to their tight aspect ratio. For example, comparing MAST to DIII-D, both with similar poloidal cross sections but aspect ratios differing by a factor of two, the curvature $\kappa = -\mathbf{b} \times \nabla \times \mathbf{b}$ with $\mathbf{b} = \mathbf{B}/B$ is 1.5 (outboard) to 5 (inboard) times higher in MAST.

Magnetic configurations:

MAST is usually operated in a DND configuration with an upper and lower X-point, as shown in Fig. 1. The two X-points, however, do not necessarily lie on the same flux surface (see Fig. 1a and c) giving rise to the distinction between lower DND (LDND, Fig. 1a), connected DND (CDND, Fig. 1b), and upper DND (UDND, Fig. 1c) configurations. Lower and upper refer to the positions of the active X-point on the LCFS. We refer to the two flux surfaces passing through the X-points as the inner and outer separatrices, shown in red (LCFS) and green in Fig.1 and define their distance as $\delta_{sep} \equiv r_l - r_u$, where $r_{l,u}$ denotes the minor radius of the separatrix passing through the lower and upper X-points respectively. Using the vertical feedback control coils, P6 (Fig. 1a), we can change δ_{sep} without changing the magnetic configuration significantly. In particular, the position of the X-points compared to the distance to the closest material surface changes by less than 2%. The average of the triangularity and elongation over all configurations is $\bar{\delta} = (0.37 \pm 0.02)$ and $\bar{\kappa} = (1.93 \pm 0.05)$. The configuration is regarded as connected if δ_{sep} at the outboard mid-plane is less than the ion Larmor radius $\rho_i \approx 6$ mm since the cross field transport is affected at least by ρ_i and the magnetic field is lowest at the outboard mid-plane. CDND is not a (power) balanced double null diverted discharge as can be seen from Fig. 2a, since the power flows preferably in the ion ∇B-drift direction, which in these experiments is directed downwards.

The magnetic configurations shown in Fig. 1 are derived from EFIT equilibrium reconstructions. To validate the accuracy of the reconstruction we use the power flow distribution to

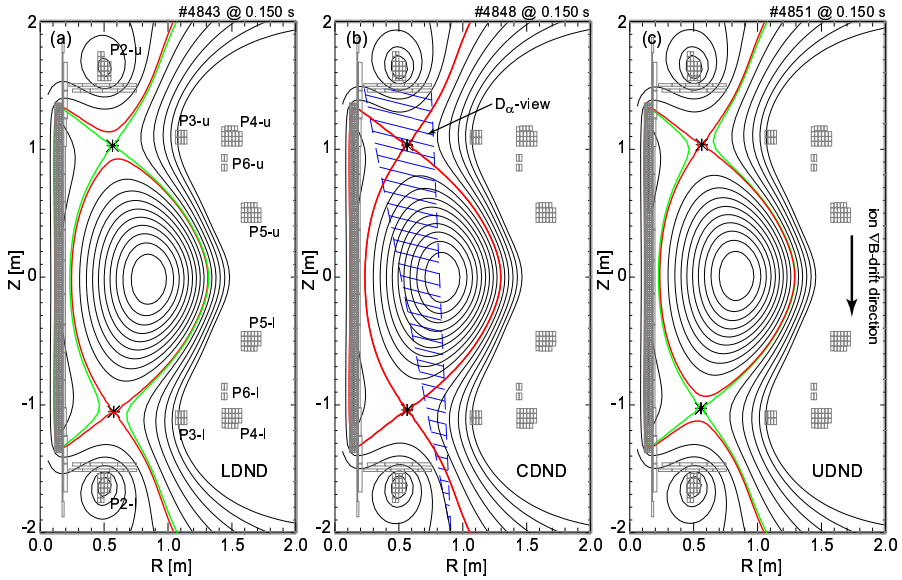

Figure 1: *EFIT reconstructions of different magnetic configurations on MAST. (a) lower (disconnected) double null diverted, (b) connected double null diverted and (c) upper (disconnected) double null diverted. The red line shows the last closed flux surface (LCFS) and the green line shows the flux surface passing through the second X-point.*

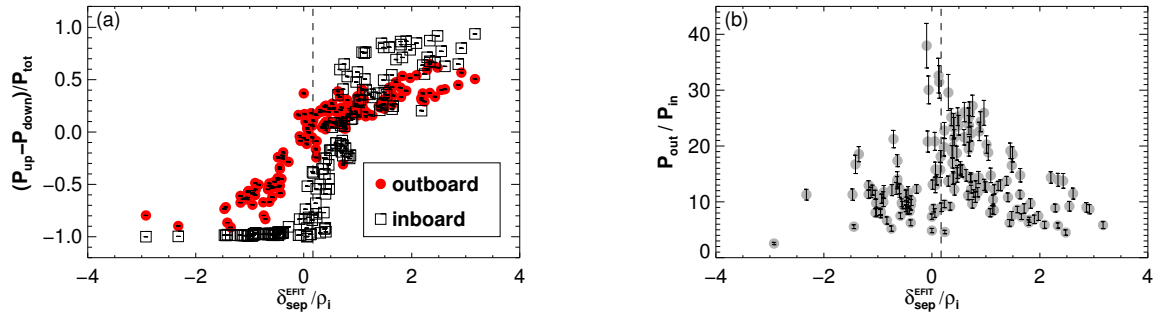

Figure 2: *(a) Up/down contrast, $(P_{\rm up}-P_{\rm down})/(P_{\rm up}+P_{\rm down})$, of power flows to outer (●) and inner (□) target plates, and (b) outboard/inboard ratio of total power flow, $P_{\rm out}/P_{\rm in}$, versus normalised separatrix separation, $\delta_{\rm sep}^{\rm EFIT}/\rho_{\rm i}$, from EFIT.*

the target plates obtained from an extensive array of Langmuir probes for an ensemble of discharges and times (see Fig. 2). The "contrast" of the power flows to the upper target plates to the power flows to the lower target plates $\Gamma_{\rm ud} \equiv (P_{\rm up}-P_{\rm down})/(P_{\rm up}+P_{\rm down})$ for the outboard and inboard sides are shown in Fig. 2a corroborating the consistency of the EFIT reconstructions. $\Gamma_{\rm ud}$ is not symmetric around $(0,0)$ reflecting the influence of the ion ∇B-drift direction on the power flow. The point of symmetry is interestingly different for the outboard and inboard side. In Fig. 2b the ratio of the outboard to inboard power flow $\Gamma_{\rm oi} = P_{\rm out}/P_{\rm in}$ is shown. Due to the unfavourable curvature and the lower magnetic field most of the power flows to the outboard side. The parallel power flow from the outboard to the inboard SOL is inhibited if $\delta_{\rm sep} = 0$, since there is no connecting flux-tube. This should lead to a peaking of $\Gamma_{\rm oi}$ at $\delta_{\rm sep} = 0$. The peak of $\Gamma_{\rm oi}$ is obtained at $\delta_{\rm sep}^{\rm EFIT}/\rho_{\rm i} \approx 0.16$ from a statistical analysis of the data shown in Fig. 2b, showing a small systematic shift equivalent to $\delta_{\rm sep}^{\rm EFIT} - \delta_{\rm sep} \approx 1$ mm. We correct for this in the following ($\delta_{\rm sep}/\rho_{\rm i} \equiv \delta_{\rm sep}^{\rm EFIT}/\rho_{\rm i} - 0.16$). This is comparable to the estimated accuracy of EFIT with respect to the separatrix separation.

H-mode quality:

In Fig. 3 are shown the traces of the divertor D_α-intensity for consecutive discharges with

different vertical positions, $Z_{\rm mag}$, of the magnetic axis. In the cases shown in Figs. 3b and 3c where $Z_{\rm mag}$ is sufficiently close to zero typical *threshold ELMs* can be seen indicating a shallow H-mode. All the discharges were sawtoothing with a similar sawtooth period of $\Delta t_{\rm st} \approx (8 \pm 1)$ ms. With both LDND (Fig. 3a) and UDND (Fig. 3d) configurations the plasma remains in L-mode.

Quantities such as $\tau_{\rm E}$ or the H-factor usually employed to define the H-mode quality are not very sensitive measures in these cases, because in a regime close to the L/H transition threshold as shown in Fig. 3 the increase in confinement is not very pronounced and hardly resolvable within the error margins of the confinement time, $\tau_{\rm E}$, calculation. A sensitive measure can be deduced, however, from the D_α emission, indicative of the particle efflux, by calculating

$$Q_{\rm H} = (D_\alpha^{\rm max}/\bar{D}_\alpha) - 1 \qquad (1)$$

in a given time interval, $\Delta t = 10$ ms, around the the single time of the high-spatial-resolution Thomson scattering (TS) measurement. Here, $D_\alpha^{\rm max}$ represents the maximum D_α-intensity in the given time period and $\bar{D}_\alpha$ the mean value. This is tracking the behaviour of threshold or type-III ELMs when the H-mode becomes deeper and the confinement better, leading to longer inter ELM periods and larger ELM events.

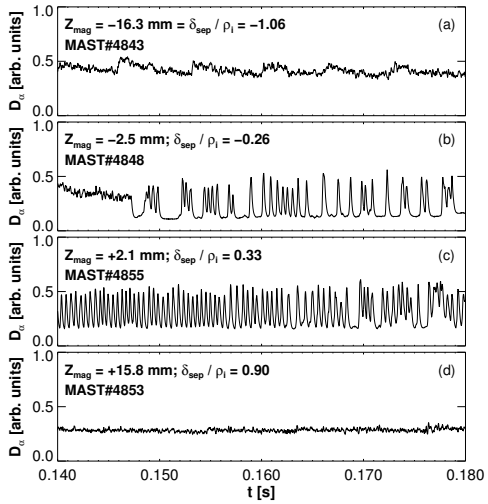

Figure 3: *Time traces of divertor D_α-intensity for similar discharges with different vertical positions.*

Q_H from Eq. (1) is plotted as a function of normalised separatrix separation in Fig. 4 for three sets of discharges with different toroidal fields, $B_0 = 0.54$ T (●), $B_0 = 0.46$ T (□), and $B_0 = 0.35$ T (◊), but similar $I_{\rm p}$ and, hence, B_θ. To estimate $\rho_{\rm i}$ at the LCFS the local TS measurement was used and $T_i \approx 1.5 \cdot T_e$ was assumed as found from modelling the MAST SOL [12]. Another good indicator for H-mode quality is the edge density gradient, $\partial n_{\rm e}/\partial r$,

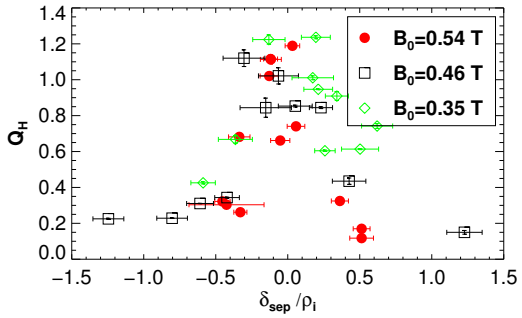

Figure 4: *Quality of H-mode versus normalised separatrix separation $\delta_{\rm sep}/\rho_{\rm i}$ for three different toroidal field values, $B_0 = 0.54$ T (●), $B_0 = 0.46$ T (□), and $B_0 = 0.35$ T (◊).*

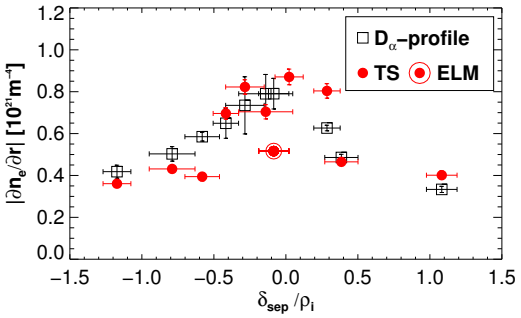

Figure 5: *Edge electron density gradient versus normalised separatrix separation from the width of the D_α emission (□) and Thomson scattering (●), ELMs are marked.*

shown in Fig. 5 for the medium field case, $B_0 = 0.46$ T, as measured from the width of the D_α-emission profile (□) [13] and from TS by fitting a modified hyperbolic tangent function to the data (●) [10]. Note, the Thomson scattering measurement on MAST is a snap-shot of the plasma of $\Delta t_{\rm ts} = 30$ ns. The marked data point shows that if the Thomson scattering measurement is during an ELM the density gradient is reduced to almost L-mode levels.

Both measures shown in Figs. 4 and 5 indicate clearly that Ohmic H-mode in these discharges is only achieved in a narrow region of $|\delta_{\rm sep}/\rho_{\rm i}| \lesssim 0.5$, i.e. in CDND configuration. Even

with auxiliary neutral beam heating up to date good H-modes on MAST are currently only observed in CDND configurations showing that CDND configurations exhibit the lowest power threshold in MAST, although an extensive assessment has yet to be performed. The similar width of the peak of Q_H (see Fig. 4) for all magnetic field settings seem to favour normalisation with ρ_i rather than the poloidal Larmor radius ρ_{pol}.

To our knowledge there is no existing theory available to explain these observations [14]. Since the phenomenon seems to be a finite Larmor radius effect, fluid based theories seem inappropriate to address the issue. We believe that the changes of gradients in the SOL and their relation to the gradients inside the LCFS are causing the differences in H-mode access because the separatrix connection is the important factor affecting mostly the SOL. The typical radial decay length in a tokamak scales roughly as $\lambda \approx \sqrt{D_\perp L_c / c_s}$, were $D_\perp$ is the cross field diffusion coefficient, L_c the parallel connection length and c_s the ion sound speed. In disconnected configurations the profiles just outside the LCFS of T_e, n_e and E_r will be flatter than in CDND due to the additional long connection length between the two separatrices. This could affect the sheared-flow just inside the separatrix in two ways. Firstly, the radial electric field E_r in the SOL, mainly determined by $\nabla_\perp T_e$, is expected to increase significantly in CDND leading to changes of $\nabla_\perp E_r$ just inside the LCFS. Secondly, according to a theory by Guzdar et.al. [15] the L/H transition is achieved if the parameter $\hat{\beta} = \beta / 2(qR/L_n)^2$ is increased above a certain critical value leading to a self organisation of the plasma edge to H-mode.

Summary:
A detailed investigation of the effect of separatrix separation on the access to H-mode in Ohmic discharges showed that H-mode on MAST is best achieved in a connected double null diverted (CDND) configuration. In these type of discharges on MAST H-mode is only reached when the distance between the two separatrices does not exceed $\rho_i/2$. The findings suggest that the lowest H-mode power threshold in spherical tokamaks will be in CDND configuration. There is no existing theory, to our knowledge, that can explain this finite Larmor radius effect. The easier H-mode access in CDND configurations, however, could result from the differences in energy and particle exhaust due to the missing parallel power flow and the additional energy and particle sinks affecting the gradients in the SOL which leads to changes of the sheared-flow just inside the LCFS. This work demonstrates the valuable insight into L/H-transition physics that can be gained on MAST.

Acknowledgements:
This work was jointly funded by the UK Department of Trade and Industry and EURATOM.

References:

[1] F. Wagner, G. Becker, *et al.*, Phys. Rev. Lett. **49** (1982).
[2] F. Wagner, J. Baldzuhn, *et al.*, Plasma Phys. Control. Fusion **36**, A61 (1994).
[3] R. J. Akers, G. F. Counsell, *et al.*, Phys. Rev. Lett. **88**(3) (2002).
[4] R. Maingi *et al.*, Phys. Rev. Lett. **88**(3) (2002).
[5] ASDEX-Team, Nucl. Fusion **29**(11), 1959 (1989).
[6] ITER-Team, *ITER Physics Basis* (Nuclear Fusion, 1999), vol. 39, chap. 2, pp. 2175–2249.
[7] T. Carlstrom, P. Gohil, *et al.*, Plasma Phys. Control. Fusion **36**, A147 (1994).
[8] G. M. Staebler and F. L. Hinton, Nuclear Fusion **29**(10), 1820 (1989).
[9] J. Cordey, W. Kerner, *et al.*, Plasma Phys. Control. Fusion **38**, 1905 (1996).
[10] R. J. Groebner and T. N. Carlstrom, Plasma Phys. Control. Fusion **40**, 673 (1998).
[11] T. N. Carlstrom, R. J. Groebner, *et al.*, in *Bulletin of the American Physical Society* (2001), vol. 46.
[12] A. Kirk, W.-J. Ahn, *et al.*, in *28th European Physical Society Conference on Controlled Fusion and Plasma Physics* (European Physical Society, Europhysics Letters, 27 Rue de la Vendée, POB 69, CH-1213 Petit Lancy 2, 2001).
[13] M. Tournianski, P. Carolan, *et al.*, Nuclear Fusion **41**(1), 77 (2000).
[14] J. W. Connor and H. R. Wilson, Plasma Phys. Control. Fusion **42** (2000).
[15] P. Guzdar, R. Kleva, *et al.*, Phys. Rev. Lett. **87**(1), 15001 (2001).